



OPEN ACCESS

EDITED BY

Dongmei Xu,
Nanjing University of Information Science
and Technology, China

REVIEWED BY

Pak Wai Chan,
Hong Kong Observatory, Hong Kong
SAR, China

Fen Xu,
Chinese Academy of Meteorological
Sciences, China

Chao Chen,
Guangdong Meteorological Observatory,
China

*CORRESPONDENCE

Yi Wang,
✉ wangyi401@163.com

RECEIVED 24 April 2023

ACCEPTED 10 July 2023

PUBLISHED 28 July 2023

CITATION

Cao S, Wang Y, Tan J, Zhuang X, Lu R,
Wei F and He Y (2023), Application of
multi-source data in a tornado process in
Jiangsu province.

Front. Earth Sci. 11:1211062.

doi: 10.3389/feart.2023.1211062

COPYRIGHT

© 2023 Cao, Wang, Tan, Zhuang, Lu, Wei
and He. This is an open-access article
distributed under the terms of the
[Creative Commons Attribution License
\(CC BY\)](https://creativecommons.org/licenses/by/4.0/). The use, distribution or
reproduction in other forums is
permitted, provided the original author(s)
and the copyright owner(s) are credited
and that the original publication in this
journal is cited, in accordance with
accepted academic practice. No use,
distribution or reproduction is permitted
which does not comply with these terms.

Application of multi-source data in a tornado process in Jiangsu province

Shuya Cao^{1,2}, Yi Wang^{3,2*}, Juan Tan⁴, Xiaoran Zhuang^{1,2}, Rong Lu⁵,
Fenfen Wei¹ and Yan He^{1,2}

¹Suzhou Meteorological Bureau, Suzhou, China, ²Key Laboratory of Transportation of Meteorology CMA, Nanjing, China, ³Jiangsu Meteorological Observatory, Nanjing, China, ⁴CMA Institute for Development and Programme Design (CMAIDP), Beijing, China, ⁵Nanjing Meteorological Bureau, Nanjing, China

This paper analyzes the weather background and triggering mechanism before the occurrence of an EF3 tornado on 14 May 2021, in southern Jiangsu, using multi-source data. Results show that 1) the tornado occurred in the warm and humid area inside the low-level shear line and the inverted trough at the surface, the southeast wind field to the east of the surface convergence line and high value area of water vapor flux on the left side of low altitude jet axis exit zone. 2) The intensity of the heavy rainfall supercell storm was strengthened after entering the Taihu Lake, and mesocyclones were detected with decreasing heights and increasing shear strengths which leading to the formation of the tornado parent storm. Tornado vortex storm bottom height dropped to 0.3km, the shear value increased to $169.1 \times 10^{-3} \text{ s}^{-1}$, strong echoes above 60 dBZ reached to the ground, the difference between the lowest elevation Radial velocity (LLDV) and the maximum Radial velocity (MXDV) reached up to the largest value when tornado occurred. 3) The strong convergence of the ground and the enhancement of mesoscale frontal zone resulted in the strong development of thunderstorm cells. The deep rear inflow behind the heavy precipitation supercell storm passed through the stratiform cloud area and produced strong updraft due to the convergence of wind direction and wind speed. The updrafts generated vertical vorticity under the influence of wind shear, which was further stretched in the middle layer of the troposphere to form the core of the tornado. 4) The flat underlying surface, abundant water vapor, lake surface thermal boundary, and strong wind convergence on the east bank of Taihu Lake provided favorable conditions for the occurrence of the tornado. The centers of the mesocyclones in the lower and middle layers were close to each other in the horizontal direction, which provided stable and vertical updrafts for the mesocyclones and strengthened the suction effect of the mesocyclones on the low-level vortices, facilitating the formation of the tornado.

KEYWORDS

tornado, heavy rainfall supercell storm, TVS, dual-polarization Doppler weather radar, lowest elevation radial velocity (LLDV)

1 Introduction

Tornadoes are highly destructive, small-scale convective weather phenomena accompanied by short-term heavy rainfall, thunderstorm winds, hail, and other severe convective weather causing serious casualties and losses. The diameter of a tornado is generally below 100 m, strong tornado can reach several hundred meters to about 1 km

(Bates, 1968; Fujita, 1971; Brown et al., 1978; Davies Jones et al., 2001; Doswell III, 2001). Tornadoes include supercell tornadoes and non-supercell tornadoes (Browning and Foote, 1976; Fujita, 1987). Supercell tornadoes are produced by supercell thunderstorms and are usually associated with mesocyclones. Fujita (1963) first proposed the concept of a mesocyclone, which is represented as positive and negative velocity pairs not far apart along the azimuth direction on radial velocity plot, typically with a scale of less than 10 km. Sustained mesocyclones are easily triggered to cause tornadoes under the environment of large 0–1 km vertical wind shear and low lifting condensation level (Ray et al., 1975; Lemon and Doswell III, 1979; Moller et al., 1994; Doswell III et al., 1993; Craven and Brooks, 2004). When conducting statistical research on strong tornadoes in the United States, the convective modes that produce tornadoes with an EF2 level or higher are divided into three categories: the first category is relatively independent individual bodies that aggregate into discrete circular or elliptical bodies, with a maximum echo of over 50 dBZ; The second type is quasi linear convection with a main axis length exceeding 100 km and at least three times the length of the minor axis, and a common leading boundary moving in series; The third type is cluster convection where multiple monomers gather into clusters and it is difficult to distinguish whether it is discontinuous or linear. The echo area above 40 dBZ is at least 2500 km² (Grams et al., 2012). Smith et al. subdivide the three types of convective forms into five: QLCS, linear hybrid, supercell, marginal, disorganized (Smith et al., 2012). The Mesocyclone of El Reno tornado in Oklahoma, United States, In 2013, inclined northward with height (Bluestein et al., 2019).

Tornadoes are low-probability weather events in China, occurring with a frequency less than one-tenth that of the United States (Fan and Yu, 2015). However, due to the fact that the high incidence areas of tornadoes in China are mainly concentrated in densely populated and economically developed areas such as the eastern plains and the Pearl River Delta (Wei and Zhao, 1995; Fan and Yu, 2015; Yao et al., 2015; Feng et al., 2017), even weak tornado events can cause significant casualties and property damage. Therefore, Chinese meteorologists have conducted investigations and studies based on different time series and regions to analyze the characteristics and disaster damage of tornadoes in different regions of China (Xue and Yang, 2003; Xu et al., 2010; Feng et al., 2012). In recent years, FY satellite (Song et al., 2022; Shu et al., 2022; Zhang et al., 2022) and radar data assimilation (Shen et al., 2016; Shen et al., 2020; Shen et al., 2022) have been applied in monitoring and prediction of meso-scale weather system. Tornadoes in China mainly occur in the plain areas of the eastern half of the mainland, such as the Jianghuai, Huanghuai, and Northeast Plains, among which Jiangsu Province has the highest frequency of tornadoes (Feng et al., 2017; Yu et al., 2021), so many scholars have conducted research on tornadoes in Jiangsu Province. On 23 June 2016, an EF4 tornado occurred in Funing County, Yancheng City, Jiangsu Province, causing significant casualties and property losses. Zheng et al. (2016) and Zhang et al. (2016) respectively evaluated and analyzed the intensity and mesoscale characteristics of the tornado process. Wu et al. (2009) analyzed the causes of the tornado weather that occurred in Gaoyou, Yancheng, and Tianchang, Anhui on 3 July 2007, pointing out that the tilting term in the mesoscale vorticity equation was an important reason of the tornado weather. Zeng et al. (2016) synthesized and analyzed 11 tornado processes during the

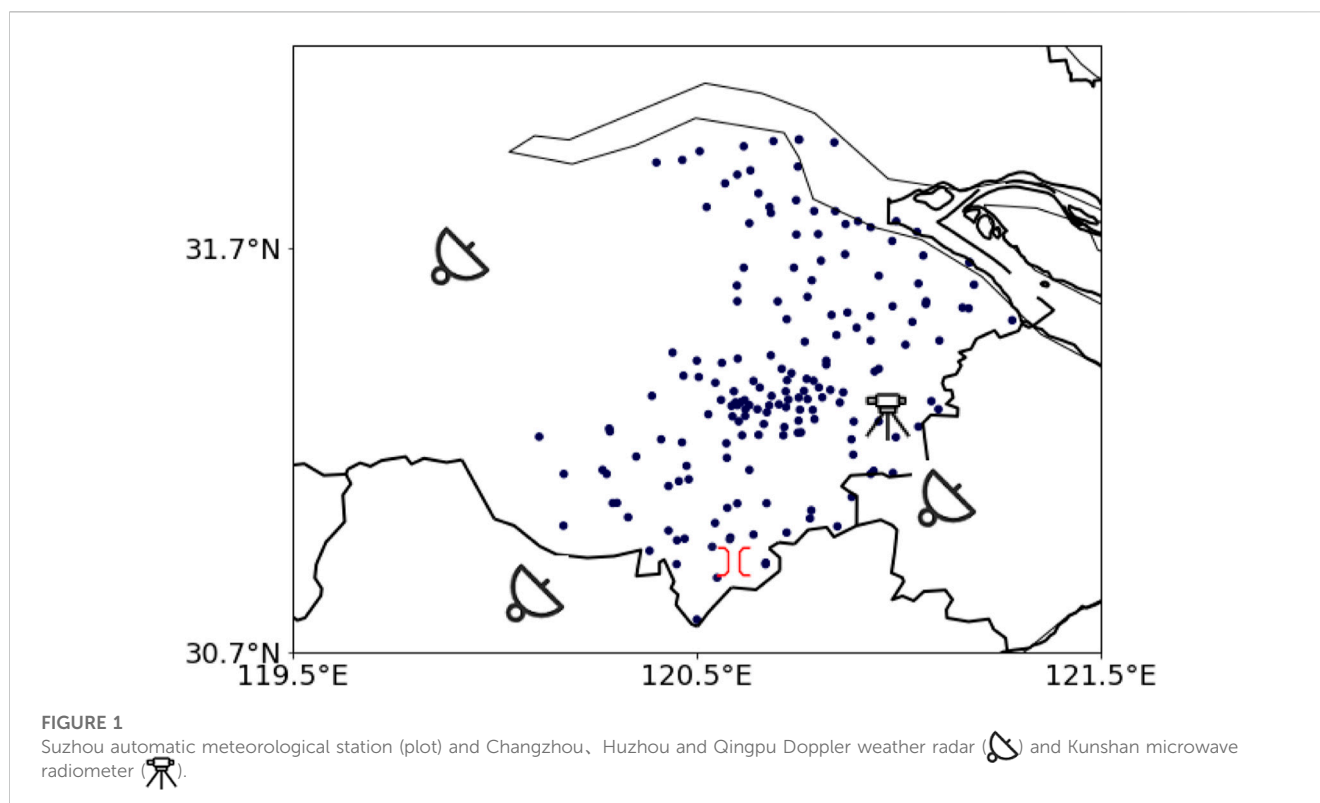
Meiyu season and identified that the area near the right side of the surface mesoscale strong cyclone, 200–300 km below the right side of the low-level mesoscale vortex in the troposphere, and the area between the left and rear sides of the low-level jet stream are areas of high concern for tornadoes. Xu et al. (2021) conducted a statistical analysis of the temporal and spatial distribution, grade distribution, weather background characteristics, and storm morphology of tornadoes in Jiangsu from 2006 to 2018, and pointed out that more than 50% of tornadoes in Jiangsu were generated in mesocyclone supercell embedded in multicell storm systems, while 30% of tornadoes occurred within quasi-linear convective systems. Wang et al. (2018) conducted a statistical analysis of mesocyclones in Nanjing radar for 10 years and found that mesocyclones lasting for three continuous sweeps and the Mesocyclone with low centroid and strong shear are conducive to tornadoes. Mu et al. (2021) conducted a detailed analysis of the EF2-EF3 tornado weather process that occurred in northern Jiangsu on 22 July 2020, and believed that when the mesocyclone bottom height was low and the shear value remained strong, combined with the evolution of the surface mesocyclone scale system, it could provide help for tornado warnings.

Domestic and foreign scholars had conducted many studies on the causes and mechanisms of tornadoes, but there were little research on the occurrence of strong tornadoes in southern Jiangsu. Therefore, this article will discuss the weather process of an EF3 level strong tornado occurred in Suzhou based on multi-source observation data, including radar, wind profile, and ground automatic station data, combined with hourly reanalysis data from the European Centre for Medium-Range Weather Forecasts (ECMWF) ERA5. This article analyzed the environmental background, key physical parameters, Supercell radar echo evolution characteristics, etc., in detail which caused the strong tornado. And the role of the Taihu Lake in maintaining and enhancing the intensity of Supercell storms was discussed, in order to provide reference for such strong tornado monitoring and early warning, and to reduce losses from tornado disasters from a meteorological perspective. However, due to insufficient monitoring density and limited detection technology, the study of tornadoes remains a challenge in small-scale synoptic studies. The following analysis is only a preliminary exploration.

2 Data and methods

2.1 Data

The data used in this article include: 1) The fifth generation global atmospheric reanalysis data ERA5 (ECMWF reanalysis v5) reanalysis data released by the European Center for Medium Range Numerical Forecasting (ECMWF), with a spatial resolution of $0.1^\circ \times 0.1^\circ$, with a time resolution of 1 h from 08:00 to 20:00 on 14 May 2021; 2) On 14 May 2021, from 08:00 to 20:00, the minute precipitation, temperature, and 2-min average wind direction and wind speed of automatic stations within the Suzhou area (Figure 1); 3) Changzhou, Huzhou and Qingpu Doppler weather radar data [operates in S band and adopts Doppler signal processing technology, frequency range is 2700 MHz–3,000 MHz, the maximum detection range is 460 km, and the detection elevation range is -1° to $+92^\circ$. The quality control of Doppler radar in this article adopts the data quality control algorithm developed by



Minshida Company (Wen et al., 2016)] from 08:00 to 20:00 on 14 May 2021 (Figure 1); 4) Kunshan microwave radiometer Data (QFW6000) from 08:00 to 20:00 on 14 May 2021 [(Kunshan Microwave radiometer adopts passive microwave remote sensing, which can detect water vapor density profile, humidity profile, temperature profile, refractive index profile and other products, and has played a certain role in weather monitoring and analysis (Mao et al., 2022), Figure 1].

2.2 Methods

Using Grads and Python mapping software, Micaps 3.2 system and meso scale analysis tools (Gao et al., 2014), weather System, dynamic conditions, and energy condition that caused the EF3 tornado process were analyzed using the synoptic method and meso scale analysis technology.

3 Overview of the process and weather background

3.1 Weather conditions

From 18:36 to 19:06 on the afternoon of 14 May 2021 (Beijing time, the same below), strong convective weather such as thunderstorms, short-term heavy rainfall, thunderstorm gusts, and small hailstones occurred successively in the jurisdiction of Suzhou, Wujiang, Wuzhong, Zhangjiagang, and Changshu in Jiangsu Province.

A total of 33 stations in the city had hourly rainfall intensity exceeding 20mm, with a maximum hourly rainfall intensity of 51.1 mm (from 18:00 to 19:00 in Daxin Town, Zhangjiagang). Thunderstorm gale of level 8 or above were recorded at 9 stations, with the largest thunderstorm gale of 31.9 m/s (level 11) occurring at Xiaoleishan in Taihu Lake. Around 19:00, a strong EF3 tornado with a maximum wind force of 17 hit Shengze Town in Wujiang District, Suzhou City.

3.2 Tornado intensity and path information

The expert team of the Jiangsu Provincial Meteorological Bureau organized a disaster investigation team to conduct a disaster investigation on site for the first time on the night of the 14th, collecting relevant disaster evidence through aerial photography, photography, visiting villagers, and collecting videos. According to the comprehensive analysis and judgment of the national and provincial expert groups in combination with the weather situation and the actual data of the observation station, the tornado occurred at about 19:00 in Shengze, Wujiang City. The maximum wind force in the tornado center was 17, and the level was EF3. The main impact path of the tornado in Jiangsu Province began to form around 18:50 near Hehua Village, Shengze Town, Wujiang District, Suzhou City, and dissipated near Xiangjiabang, Tianning Town, Jiashan County, Zhejiang Province at approximately 19:10, lasting for about 20 min. The movement path of the tornado is about 19 km, with a length of about 8 km within Jiangsu Province. The obvious damage width is about 100 m, and the severe damage width is about 50 m (Figures 2A–E).



FIGURE 2
Tornado disaster situation (A–D) of Jiangsu Shengze on 14 May 2021 and Tornado Movement Path (E).

3.3 Tornado disaster situation

The Wujiang Shengze tornado caused a total of 4 deaths, 19 minor injuries, and 130 minor injuries on May 14th. Power facilities and multiple houses were damaged, with 84 households and an area of 1,500 square meters damaged; 17 damaged enterprises, with a damaged area of 13,000 square meters.

3.4 Weather background

At 08:00 on the 14th, Jiangsu was located in the divergence zone on the right side of the 200 hPa high-altitude jet stream axis. The 120°E ridge line of the 500 hPa Western Pacific Subtropical High (hereinafter referred to as the subtropical high) was located near

20°N with low vortices generated in the mid latitude 90°E plateau. The subtropical high has weakened due to the eastward movement of the plateau trough. Most of Jiangsu was located in front of the trough and in the warm and humid southwest airflow around the periphery of the subtropical high, with a warm ridge extending eastward and northward in the north of Zhejiang, which in conjunction with the warm and humid southwest jet in front of the trough to continuously transport water vapor and unstable energy to southern Jiangsu. There was a southwest-southeast shear line existed between 32 and 33°N, and southern Jiangsu was located in the warm southwest jet stream on the south side of the warm shear. In the afternoon, the southwest jet near 30°N further strengthened and extended eastward, and the southwest wind speed at 850 hPa in southern Jiangsu increased from 12 m/s–18 m/s. The low-level jet axis was located in northern

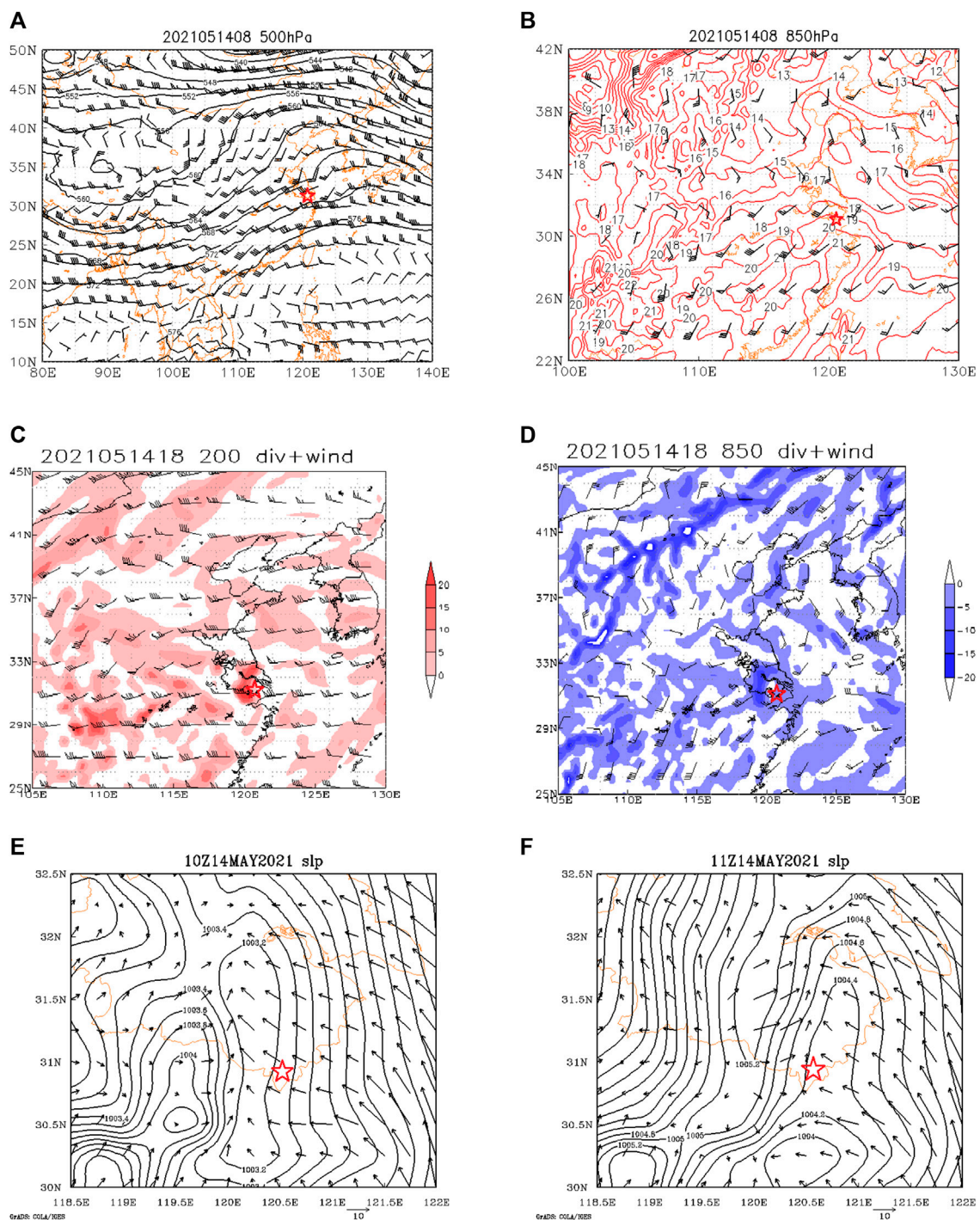


FIGURE 3
 Altitude and wind field at 500 hPa (A) and 850 hPa (B) at 08:00 BT on 14 May2021; Divergence and wind field at 200 hPa (C) and 850 hPa (D) at 18:00 BT on 14 May2021; pressure and wind field on the ground at 18:00 BT (E) and 19:00BT (F) on 14 May2021.

Zhejiang, with a wind speed of 20 m/s. The divergence in the upper layers, the shear line in the low-levels, and the enhancement of the jet stream formed a circulation background conducive to the development of tornadoes (Figures 3A–D).

Under the combined action of positive vorticity advection and warm moist advection in front of the trough, the surface pressure

decreased, and a low-value system developed. Suzhou was located at the top of the low-pressure inverted trough, and the southeast airflow on the north side of the inverted trough transported water vapor from the sea to Suzhou. The temperature and dew point temperature difference on the ground was low, indicating high humidity. At 18:00, a north-south convergence line developed on the ground.

TABLE 1 Environmental parameters of Hangzhou Station at 08:00 and 20:00 BT on 14 May2021.

	CAPE (J/kg)	CIN (J/kg)	K (°C)	SI	T850-500 (°c)	0–1 km wind shear (m/s)
08:00BT	391	195	37.5	-3.7	28	14
20:00BT	2,334	0	41.3	-3.5	30	16

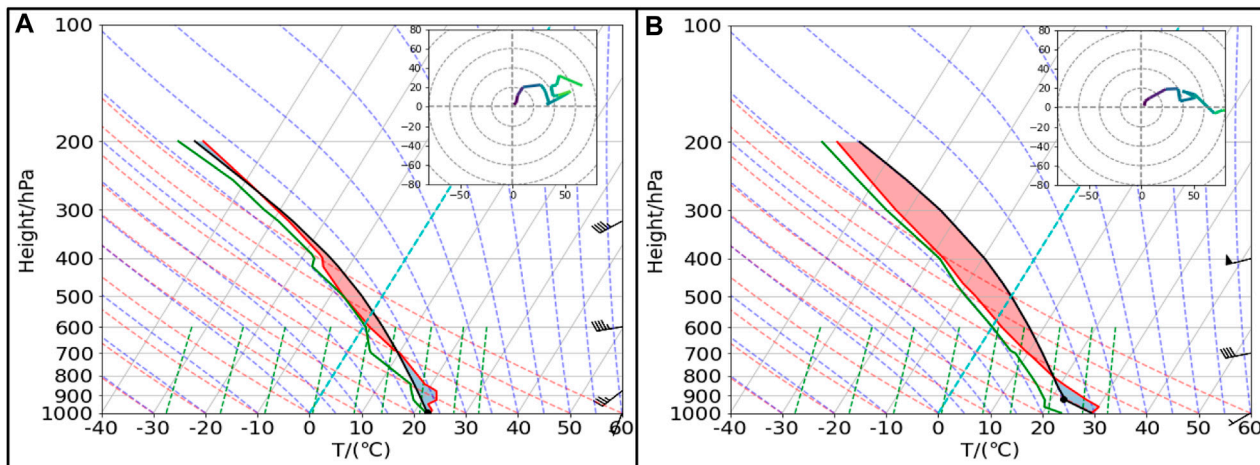


FIGURE 4
Sounding map of HangZhou station at 08:00 (A) and 20:00 (B) BT on 14 May2021.

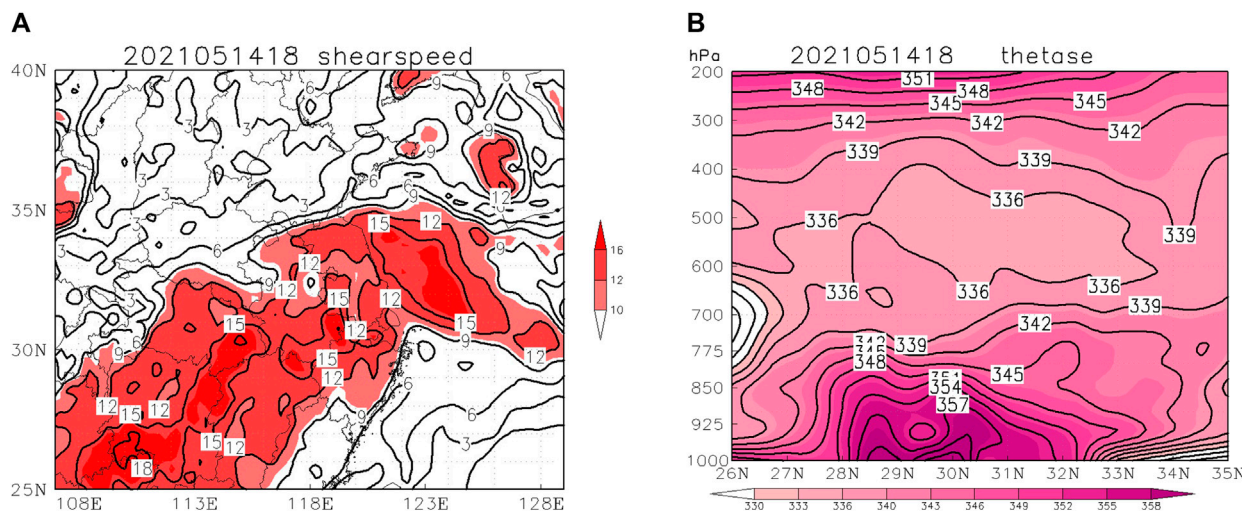


FIGURE 5
0–1 km vertical wind shear (A) and pseudo-equivalent potential temperature (unit:K) (B) at 18:00 BT on 14 May2021.

During the eastward movement of the convergence line, the intensity of the convergence line continued to strengthen. Tornado occurred in the warm and humid area inside the low-level shear line and the inverted trough at the surface, the southeast wind field to the east of the surface convergence line and high value area of water vapor flux on the left side of low altitude jet axis exit zone (Figures 3E, F).

3.5 Unstable atmospheric structure

At 08:00 on the 14th, the sounding at Hangzhou station showed (Figure 2A; Table 1) that the Convective Available Potential Energy (CAPE) was 391 J/kg, the Convective Inhibition (CIN) was 195 J/kg, the K-index was 37.5°C, and the Showalter Index (SI)

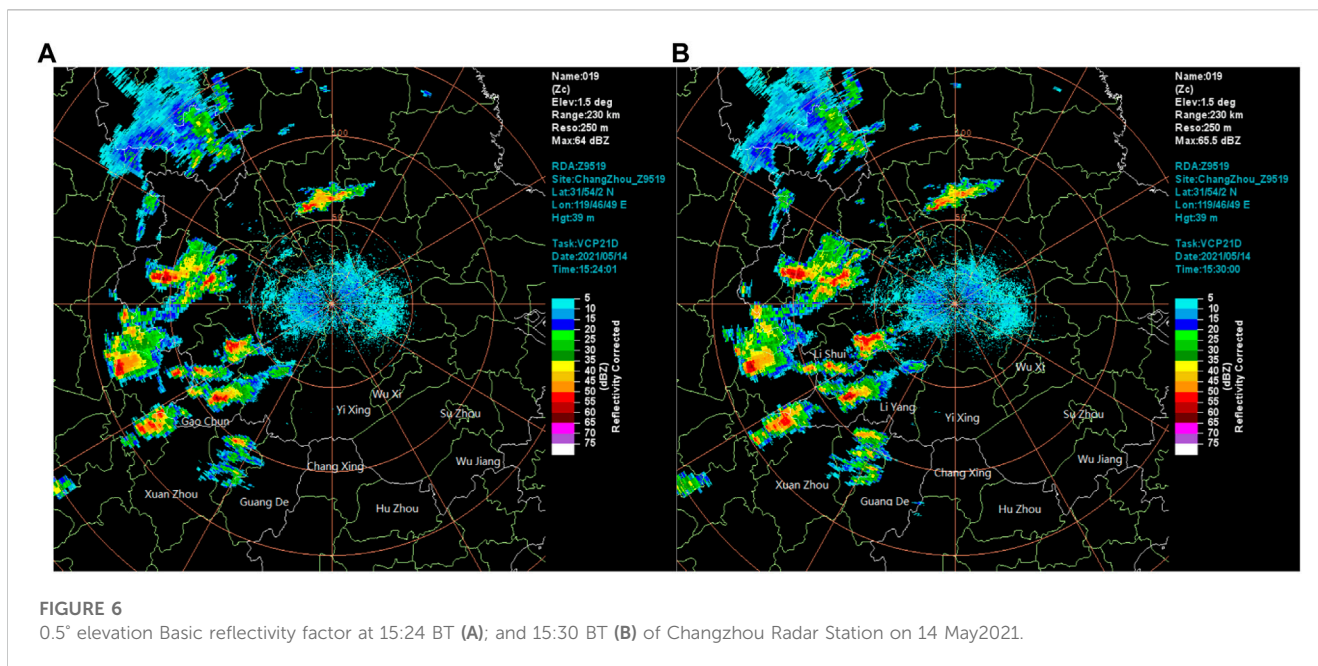


FIGURE 6
0.5° elevation Basic reflectivity factor at 15:24 BT (A); and 15:30 BT (B) of Changzhou Radar Station on 14 May2021.

was -3.7 indicating the presence of strong unstable energy in the atmosphere. By 20:00, the CAPE rapidly increased to 2334 J/kg (Figure 4B), the CIN decreased to 0 J/kg, and the K-index was 41.3°C , the temperature difference between 850 and 500 hPa was close to 28°C , indicating a further increase in unstable energy in the atmosphere. Compared with the physical quantity index when tornado occurred in Jiangsu Province, that is the CAPE value of $1,000$ J/kg, K index of 30°C , SI index of 0.5°C , the temperature difference between 850 and 500 hPa of 25°C , each physical quantity value during this weather process exceeded the threshold for tornado occurrence in Jiangsu Province. The temperature lapse rate from the surface to 925 hPa was close to dry adiabatic lapse rate. The temperature-dew point difference near surface was less than 2°C , indicating that the surface was close to saturation, and both the temperature and humidity vertical lapse rates were large. There was a dry layer with a temperature-dew point difference greater than or equal to 5°C between 700 and 450 hPa. At 14:00, the temperature-dew point difference in the middle layer further increased, presenting an overall bell mouth structure of “dry and cold at the top, warm and humid at the bottom”, with the lifting condensation level near the surface, which was conducive to the triggering of deep moist convection.

On the sounding map of Hangzhou at 08:00, there was a consistent southwest wind above the ground (Figure 4A). The vertical wind shear was mainly characterized by wind speed shear, and the wind field near the ground was weak, with a wind speed of only m/s, approaching calm winds. The wind speed at 700 hPa was 18 m/s, and the wind speed from 650 hPa to 400 hPa was 20 m/s. At 18:00, the horizontal distribution of vertical wind shear at 850 hPa in southern Jiangsu showed that both 0–1 km and 0–6 km vertical wind shear had large centers (Figure 5A), and the center values exceeded 18 m/s. The vertical wind shear at deep-layer and low-level reached a moderate strength, and strong 0–1 km vertical wind shear was conducive to the occurrence of

tornadoes, with a storm-relative environmental helicity (SREH) reaching 264 m^2/s^2 .

From the 850 hPa pseudo-equivalent potential temperature (θ_{se}) at 18:00 on the 14th (Figure 5B), the northeast southwest direction high-value belt of θ_{se} on the northwest side of the subtropical high extended to the southern part of Jiangsu Province, with a center value of over 351 K. Tornadoes occurred on the warm and humid side of the θ_{se} frontal zone. On the vertical profile of pseudo-equivalent potential temperature, the frontal surface over southern Jiangsu ($30\text{--}30^{\circ}\text{N}$) tilted with altitude, with a unstable layer structure where θ_{se} decreased with altitude below 500 hPa, reflecting the characteristics of atmospheric tilt, which was conducive to the occurrence and development of mesoscale convective systems. At 16:00 on the 14th, water vapor strongly converged in the southeastern part of Jiangsu Province, with abundant warm and humid airflow transport and accumulation, making the lower atmosphere in southern Jiangsu very humid, providing favorable warm and humid environment for the occurrence and development of tornadoes (Figure omitted).

4 Characteristics of the evolution of the supercell thunderstorm

4.1 Initial stage of the convective storm

At 15:24 on the 14th, there were several new formed convective cells arranged in a north-south direction in the area between Xuancheng and southern Nanjing with loose organizational structure. The convective cell in the southern part of Nanjing had a central intensity exceeding 60 dBZ, and moved in the northeast direction with obvious backward propagation (Figure 6A). At 15:30, a mesocyclone was detected at the rear of the convective cell. Later on,

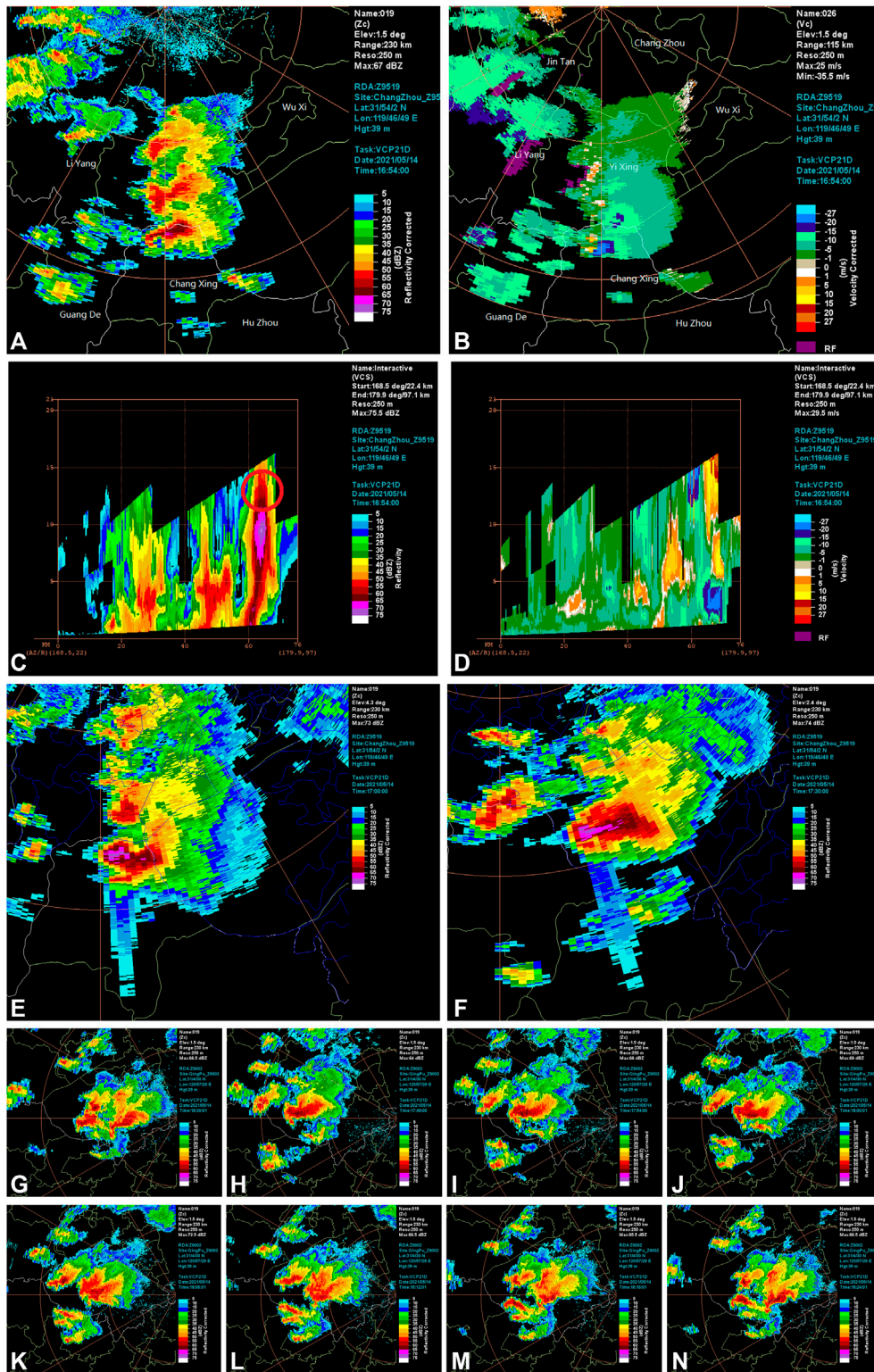


FIGURE 7
 1.5° elevation Basic reflectivity factor (A) Radial Velocity (B) Reflectivity Factor Profile (C) Radial Velocity Profile (D) at 16:54 BT of Changzhou Radar Station on 14 May 2021.; 4.3° elevation Basic reflectivity factor at 17:00 BT (E) and 2.4° elevation Basic reflectivity factor at 17:30 BT (F) of Changzhou Radar Station on 14 May 2021.; 1.5° elevation Basic reflectivity factor at 17:48 BT (G) at 17:54 BT (H) at 18:00 BT (I) at 18:06 BT (J) at 18:12 BT (K) at 18:18 BT (L) at 18:24 BT (M) at 18:30 BT (N) of Qingpu Radar Station on 14 May 2021.

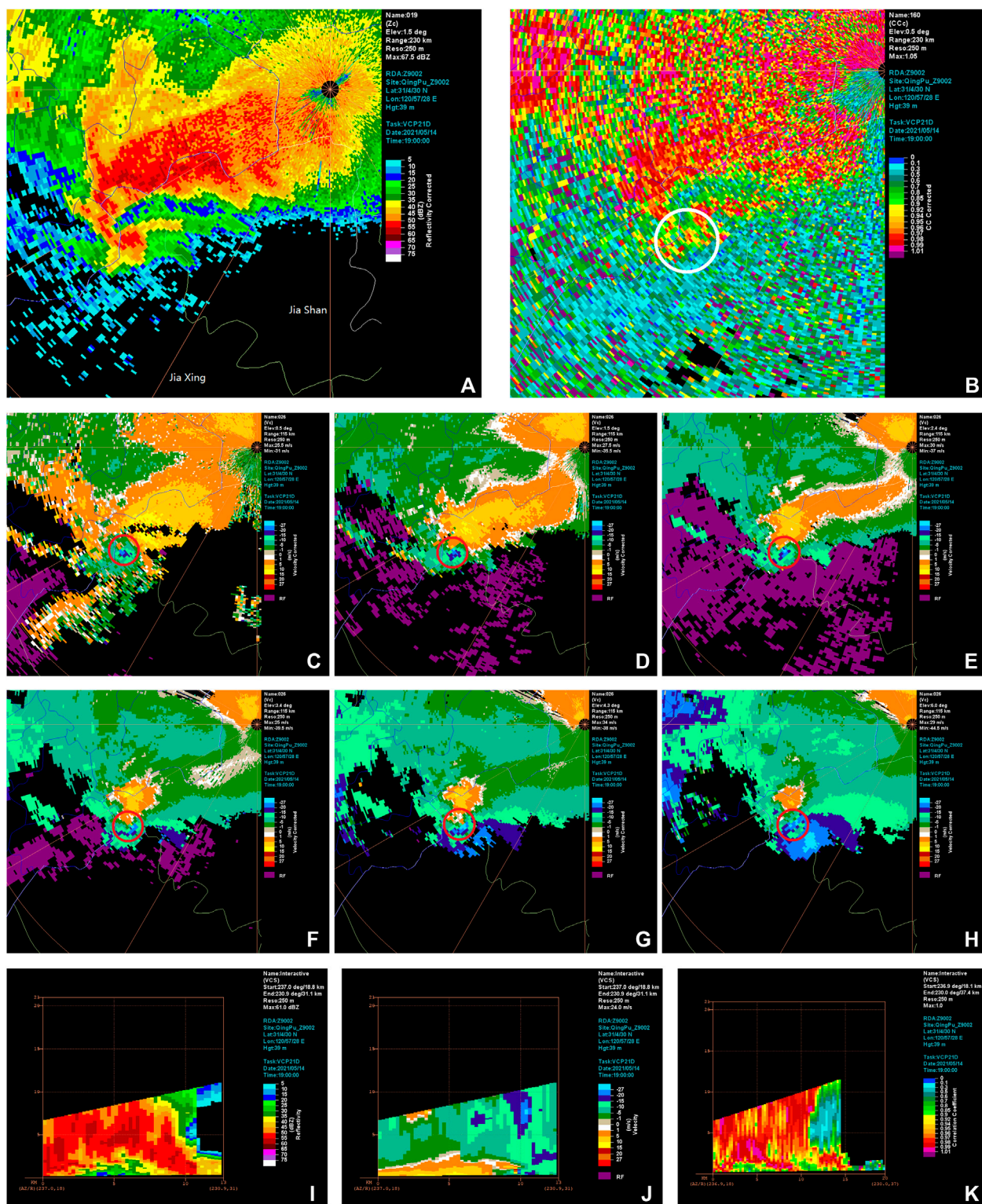


FIGURE 8 1.5° elevation Basic reflectivity factor (A) and 0.5° elevation CC (B) at 19:00 BT of Qingpu Radar Station on 14 May2021.; 0.5° (C) 1.5° (D) 2.4° (E) 3.4° (F) 4.3° (G) 6.0° (H) elevation Radial Velocity at 19:00 BT of Qingpu Radar Station on 14 May2021.; Reflectivity Factor Profile (I) Radial Velocity Profile (J) CC Profile (K) of Qingpu Radar at 19:00 BT on 14 May2021.

the north-south convective cells gradually formed an organized structure and became arranged in strips. Among them, the convective cell located in the north of Huzhou rapidly

strengthened in intensity, and the maximum central intensity reached 65 dBZ before entering Taihu Lake. Mesocyclones were detected at multiple times since 16:36 (Figure 6B).

TABLE 2 Parameters of Qingpu radar TVS on 14 May2021.

Time/BT	Bottom height/km	Top height/km	Shear value/(10^{-3} /s)	Maximum shear height/km	LLDV/(m/s)	MXDV/HGT/km
17:18	1.3	7.6	66.5	6.3	24	56.0/7.6
17:36	1.2	7	42.3	5.8	19	30.5/3.9
17:42	1.1	6.6	32.4	5.5	23	22.5/1.1
17:48	1.1	6.3	31.2	5.2	20	21.5/6.3
17:54	0.9	5.5	41.6	4.6	20	26/2.2
18:00	0.9	5.4	44.6	4.5	18	26.0/5.4
18:06	0.9	5.4	56	4.5	13	30.5/4.2
18:12	0.7	4.7	53.5	4	12	28/4.7
18:24	0.6	4.1	55.2	3.5	19	25.5/3.3
18:36	0.5	3.3	73.4	2.8	11	26.5/3.3
18:54	0.4	2.1	165.7	1.7	46	46/0.4
19:00	0.3	2.1	169.1	1.8	16	41/1.3

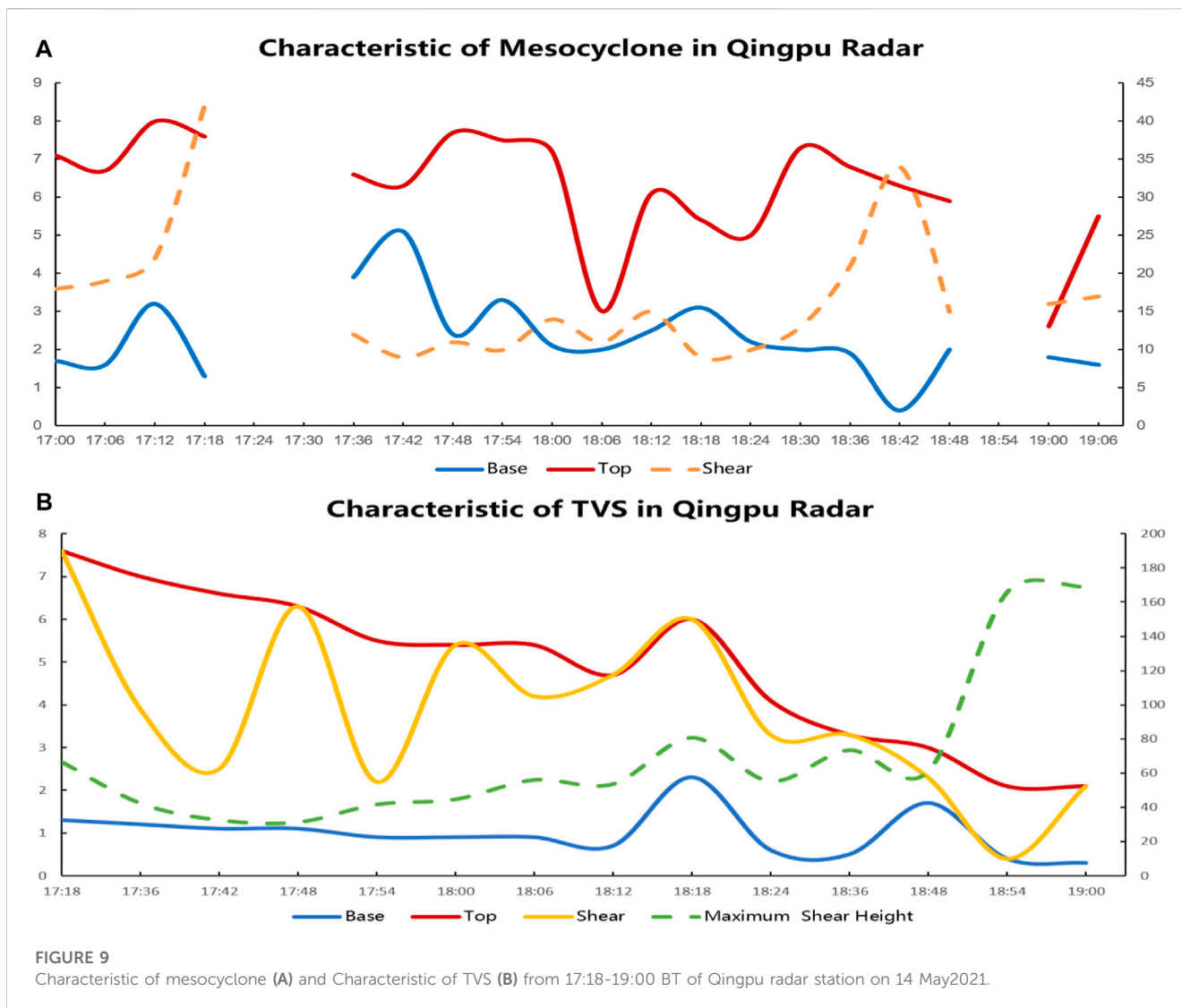
4.2 Development stage of the supercell thunderstorm

At 16:54, the convective storm entered the Taihu Lake Lake to maintain its development, with strong divergence at the storm top, and typical hail supercell characteristics. The hook like structure began to appear on the echo shape with obvious positive and negative velocity pairs on the radial velocity map at an elevation of 0.5° , with a rotational speed of 11 m/s (Figures 7A,B). It can be seen that echo development was vigorous, with a top height of 15 km and echo overhang on the profile. Convergence occurs in the lower layers of the storm, while strong divergence occurs in the upper layers (Figures 7C,D). After the main body of the storm entered Taihu Lake, its intensity was maintained and even strengthened, and mesocyclones were detected continuously during multiple body scans (Figures 7E,F). At 17:18, a new convective cell was triggered again in the southern part of Suzhou, with an initial central intensity exceeding 55 dBZ, and the first TVS appeared on the Qingpu radar, with a shear intensity of 66.5×10^{-3} /s, a bottom height of 1.3 km, and a maximum shear height of 7.6 km. At 17:30, when the convective storm moved to the east of the Taihu Lake, its intensity was slightly weakened, and the hook structure was not very clear, two convective echoes in the southern part of Suzhou gradually merged, and the echo range gradually expanded. At 17:36, typical supercell characteristic can be seen in the vertical profile such as echo overhang and bounded weak echo region. Three body scattering features were detected multiple body scans from 17:00 to 17:36, but disappeared at 17:42. At 17:54, the convective storm began to merge with the convection cell moved in from Huzhou. At 18:18, it merged again with the convection cell moved in from Huzhou, and the hook like structure was appeared again. The bottom height gradually decreased from 1.2 km to 0.7 km, and the shear intensity gradually increased. During the eastward movement of the intense precipitation supercell, its intensity continued to be maintained, with central intensity exceeding 70 dBZ, accompanied

by mesocyclones of multiple body scans, and continuous occurrence of TVS at seven body scans. Tornado parent vortex was formed in the heavy rainfall supercell storm (Figures 7G-N).

4.3 Mature stage of the supercell thunderstorm

At 18:30, the storm moved eastward into Wujiang, with a maximum vertical integrated liquid water content (VIL) exceeding 21 kg/m^2 , and the strong echo core shifted to the right side with increasing altitude. At 19:00, when the tornado occurred near Shengze, it can be seen from the basic reflectivity factor map of Qingpu radar at 1.5° elevation that the tornado hook structure is further clear, corresponding to the cyclonic vortices appeared in the velocity field (Figure 8A). It can be seen from the radial velocity field at 1.5° elevation that there is a corresponding cyclonic vortex near the Hook echo. Smaller scale cyclonic vortex near the Hook echo can be seen from the radial velocity diagram at $0.5^\circ - 6.0^\circ$ elevation, corresponding to the strong rotation of tornadoes. From the profile of the basic reflectivity factor, it can also be seen that strong echoes above 60 dBZ reached the ground. There were strong positive and negative velocity pairs of 20 m-s-2 and -20 m-s-2 near the ground on the radial velocity profile, and the positive and negative velocity differences reached 44 m/s, clearly indicating the characteristics of tornado grounding (Figures 8C-H). The echo top height exceeded 18 km, and the center of the echo top height was located north of the tornado occurrence site, indicating that the convective storm was tilted under the strong vertical wind shear, and the horizontal distribution of the echo top height was extremely uneven, indicating that the intensity of the updraft had a large horizontal gradient (Figures 8I,J). It can be seen from the dual polarization radar parameter CC that at 19:00, the tornado had obvious tornado debris characteristics (TDS). There was a low CC value area of 0.3–0.6 near the Hook echo, and the abnormal low CC value area can



also be seen from the CC profile, mainly due to the fact that tornadoes near the ground throw debris into the air with random directions and irregular shapes, resulting in a small correlation coefficient CC at the TDS feature (Figures 8B,K).

4.4 Mesocyclone and TVS evolution

From the evolution trend of Mesocyclone detected by Qingpu radar, it can be seen that Mesocyclone was recognized in 9 consecutive individual scans from 18:00 to 19:00, and TVS characteristics appeared in Mesocyclone, indicating the possibility of tornado gradually increased. Within 30 min before the tornado appeared, the bottom height of Mesocyclone was basically below 2 km, especially at 18:42 before the tornado appeared, the bottom height of Mesocyclone was below 1 km, and the shear strength jumped to $34 \times 10^{-3}/s$ (Figures 9A,B).

Table 2 showed the TVS characteristics identified by Qingpu radar from 17:18-19:00 on 14 May 2021, where LLDV represents the minimum elevation Radial velocity difference, MXDV represents the

maximum Radial velocity difference. It can be seen that from 18:00 to 18:48, the bottom height of TVS remained basically around 1 km, while the top height of TVS showed a continuous downward trend. At the same time, the maximum shear height rapidly decreased from 6 km to below 2 km, indicating that the tornado vortex is continuously decreasing. At 18:54 when the tornado occurred, the TVS bottom height dropped to 0.4 km and the shear rapidly increased to $165.7 \times 10^{-3}/s$. As the tornado Hook echo structure became clearer at 19:00, the TVS bottom height further decreased to 0.3 km, and the shear further increased to $169.1 \times 10^{-3}/s$, while the strongest shear height dropped to near the TVS bottom at 18:54, indicating that the tornado vortex had grounded. In summary, the low bottom height and strong shear of TVS have important indicative significance for tornado warning.

The value of the lowest elevation Radial velocity difference (LLDV) of the tornado was all more than 10 m/s from 17:18-19:00, and more than 20 m/s at most times, reaching a maximum of 46 m/s at 18:54 when the tornado occurred. The maximum Radial velocity difference gradually increased before the tornado occurred, and also reached the maximum value (46 m/s) at 18:54 when the tornado

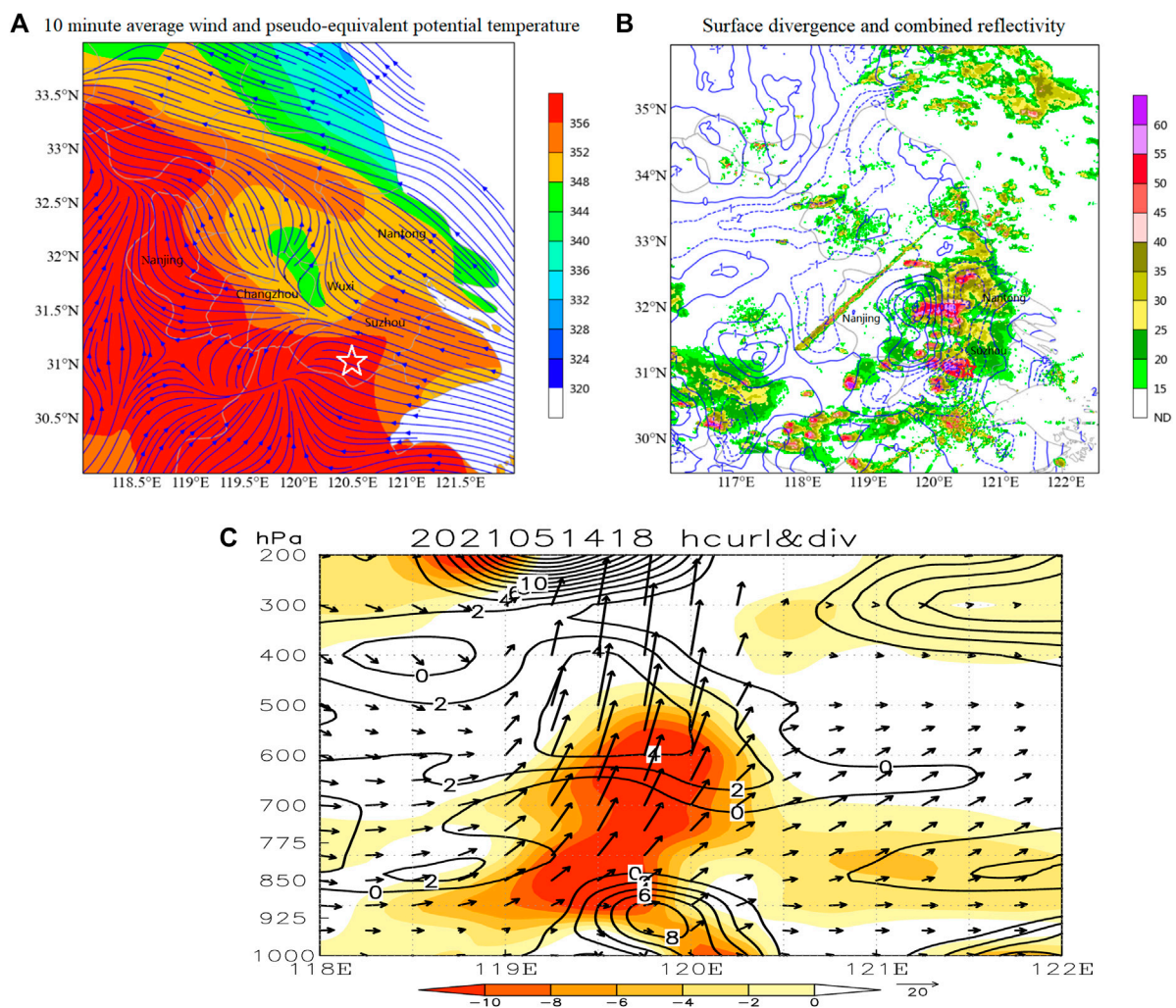


FIGURE 10

10 min average wind and pseudo-equivalent potential temperature (A) surface divergence and combined reflectivity (B) vertical velocity (vector), vorticity (contour), and divergence (shaded) profiles along 30.8° E (C) at 18:00 BT on 14 May 2021.

occurred. The height of the maximum speed difference gradually decreased, reaching a minimum value of 0.4 km at 18:54 when the tornado occurred, and the height of the maximum speed difference was close to the ground. It can be seen that the tornado occurred at the moment when the difference between the lowest elevation Radial velocity (LLDV) and the maximum Radial velocity (MXDV) reached up to the largest.

5 Triggering and formation mechanisms

5.1 Surface convergence

The surface convergence line is an important system for the occurrence and development of tornadoes. At 18:00 on the 14th, the temperature in most parts of Suzhou was between 29°C and 30°C, and the thermodynamic conditions were good. There was a surface convergence line formed by a northerly wind and a southeasterly

wind and a convergence center with divergence of $-40 \times 10^{-6}/s$ in Huzhou to the southwest of Suzhou. The northerly wind increased on the north side of the convergence line, the convergence center strengthened, and the divergence increased to $50 \times 10^{-6}/s$. The strong convergence and the strengthening of the mesoscale front zone made the thunderstorm cell develop strongly, and finally develop into a tornado parent supercell storm. At 19:00, there were two convergence centers in the north and south of Suzhou, and the convergence intensity was reduced, indicating that the organized structure of the storm began to weaken. At 20:00, the storm continued to move eastward and gradually moved away from the surface convergence line. Suzhou turned into a divergence field, and the surface of Wujiang is dominated by northeast winds, and the severe convective weather ended (Figures 10A,B).

At 18:00 on the 14th, there was strong convergence below 500 hPa in southern Jiangsu, with a convergence center value exceeding $-10 \times 10^{-4}/s$, which greatly enhanced the updraft, with a whole layer of upward motion from 850 hPa to 200 hPa in southern Jiangsu. The updraft generates vertical vorticity under the effect of wind speed and wind direction shear, which started

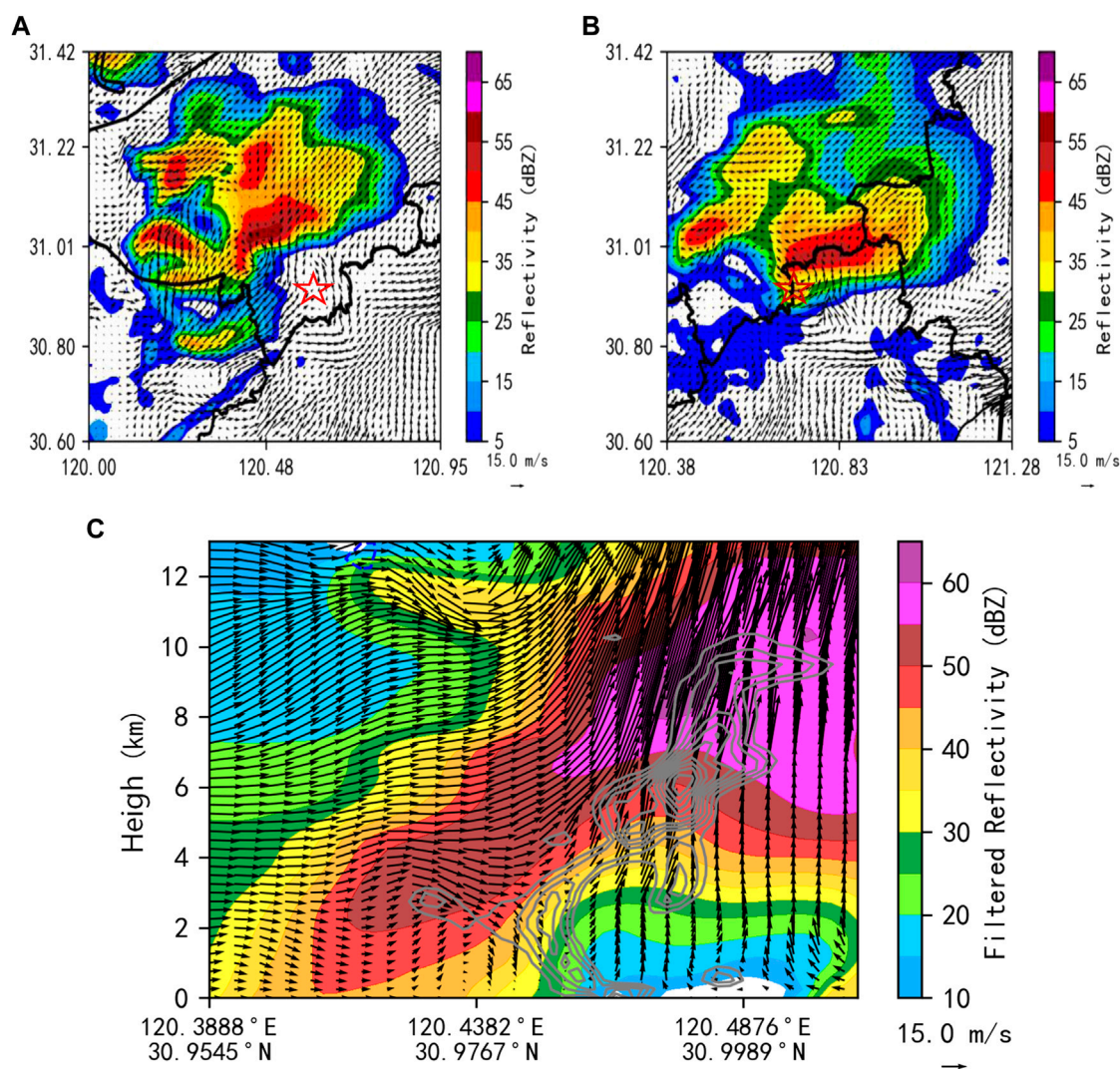


FIGURE 11

Superposition map of reflectivity factor ZH and 1 km wind field at 18:24 BT (A) and at 18:48 BT (B); ZH Profile and Wind Field Overlay Map at 18:24 BT (C) on 14 May2021.

to rotate in the horizontal direction, and the strong vertical motion gradient caused the wind field to a rapid increase in the cyclonic rotation of the wind field. There was a deep positive vorticity center below 850 hPa in the vortex field, which matched the strong upward motion area. The low-level cyclonic vorticity developed strongly before the tornado occurred, and the stronger the horizontal vorticity field in the lower troposphere, the stronger the vertical vorticity converted into the updraft, which was further stretched by the updraft to form a tornado (Figure 10C).

5.2 Rear inflow

Using the multi-radar inversion technology based on three-dimensional variational techniques developed by Potvin et al.

(2012), the wind field structure in the thunderstorm before the tornado occurred was inverted. It can be seen that there was a mesoscale front zone on the north side of the convergence line. At 18:24 as the Huzhou cell moved northward and merged with the Suzhou cell, the frontal inflow rapidly increased, forming a hook structure, and vortex pairs appeared near the hook structure. At 18:54, there was a cyclonic rotation of the wind field in the front of the middle-γ scale supercell to the northwest of Wujiang, which progressed into the convective system under the convergence airflow, and enhanced the vertical vorticity in the middle-γ scale supercell area, promoting the rapid strengthening of the middle-γ scale supercell in the middle troposphere to form the tornado core, and the rapidly enhanced supercell finally led to the tornado process (Figures 11A,B).

The generation of a tornado is a prerequisite for the formation of a low-level mesocyclone, and the formation of a low-level

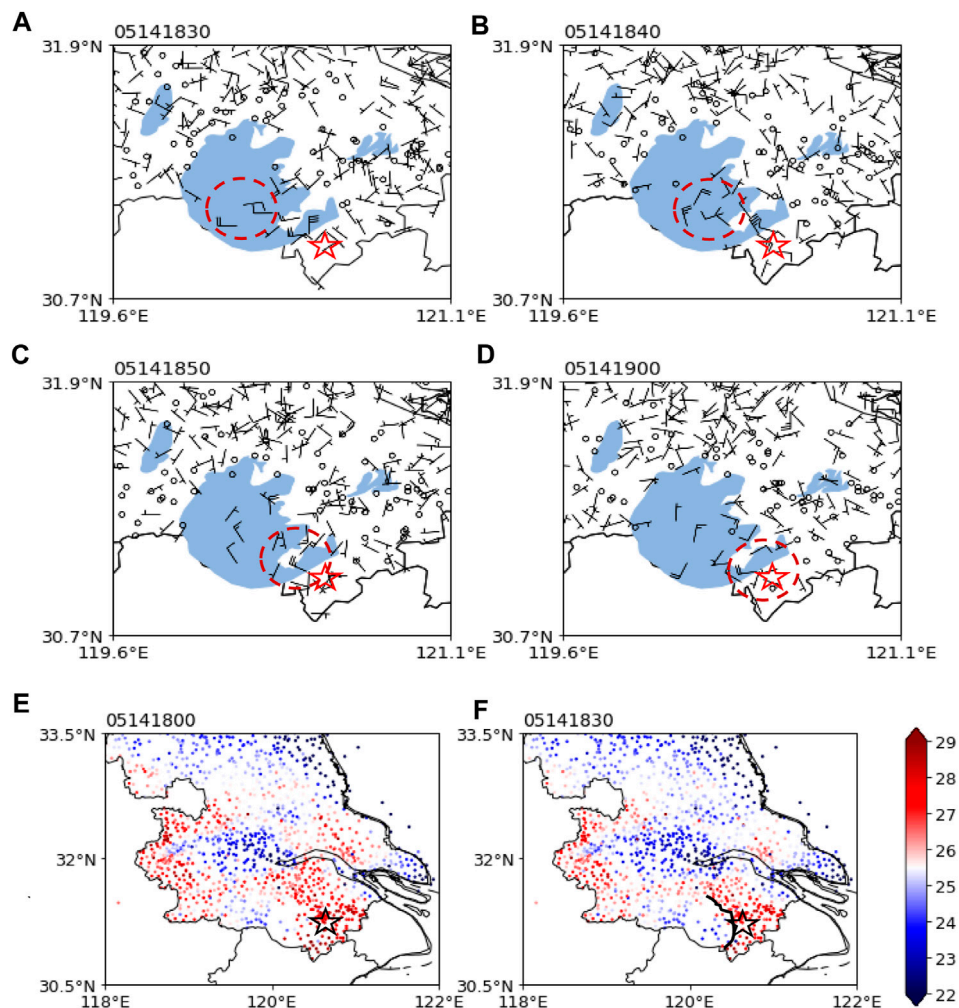


FIGURE 12
Wind field of Surface automatic weather station in southern Jiangsu (blue shaded: Taihu Lake) at 18:30 (A) 18:40 (B) 18:50 (C) 19:00 (D) BT; Surface temperature distribution in central and southern Jiangsu at 18:00 (E) 18:30 (F) BT on 14 May2021.

mesocyclone is related to the rear inflow. When the Huzhou cell moved near the surface convergence line, the outflow boundary of the storm met the surface convergence line, which enhanced the uplift effect. Taking a vertical profile along the maximum rear inflow of the convective storm, it can be seen that the flow field is mainly composed of system-relative flow from back to front. During the development stage of the heavy rain supercell storm, there is a deep rear inflow from 0 to 12 km in the rear of the storm. When it passes through the stratiform cloud area, strong updrafts are produced due to the convergence of wind direction and speed, and the vertical vorticity is generated under the strong wind shear, which starts to rotate horizontally (Figure 11C).

5.3 Analysis of Taihu Lake's role

The occurrence of tornadoes is closely related to the properties of the underlying surface, and they are more likely to occur in flat areas near rivers and lakes (JIANG L et al., 2022). The tornado

occurred in Shengze, Wujiang, 20 km away from the east bank of the Taihu Lake. On the one hand, the broad surface of Taihu Lake, provided a flat underlying surface for the occurrence of the tornado, and the abundant water vapor near the lake surface provided the necessary conditions for maintaining and strengthening the tornado's parent storm. On the other hand, the east bank of Taihu Lake is a plain, and the wind is mainly westerly in this region at 18:00 on the 14th. The wind speed over the lake is significantly larger than that on the land, and wind convergence forcing uplift near the east bank of Taihu Lake. At 18:30, a mesoscale cyclonic rotation appeared in the east part of Taihu Lake along the convergence line, and the cyclonic wind field was weak at this time. During the eastward movement of the cyclonic wind field at 18:40, its intensity rapidly increased and its range narrowed, forming a small-scale vortex in the south of Wujiang on the southeast coast of Taihu Lake. At 18:50, the wind direction recorded by the four nearest automatic stations showed a convergence toward the tornado's location. This means that the tornado's location was in the upward motion area at the center of the convergence during this

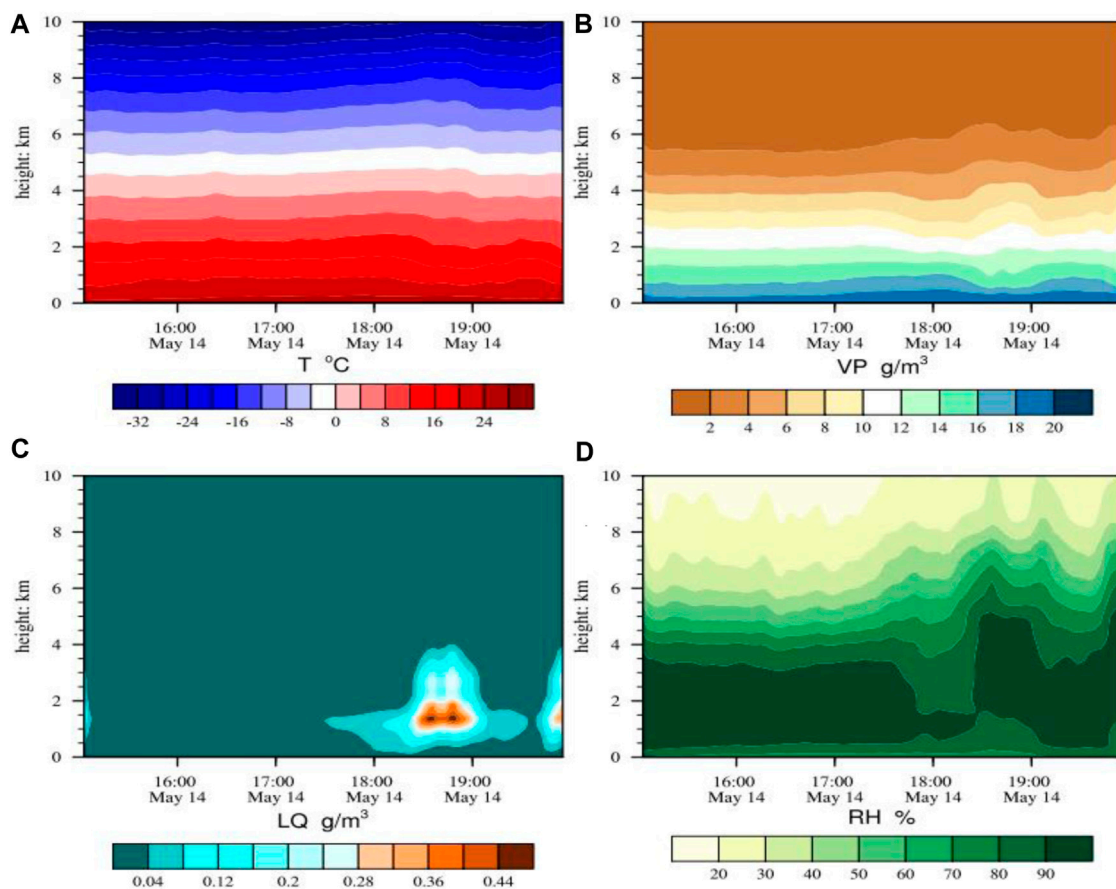


FIGURE 13

Microwave radiometer temperature profile at Kunshan Station (A); Water vapor density (B); Liquid water (C); Relative humidity (D) profile at 15:00–20:00 BT on 14 May2021.

period. When the vortex met the upward motion area of convergence, it was stretched, causing the rotation to accelerate and forming the tornado (Figures 12A–D).

When the temperature between the cold pool and the environment is suitable (less than 4°C), and the ground outflow generated by the cold pool and the environmental inflow reach a balance, the frontal tilt is small, and the centers of the lower and middle-layer mesocyclone are close to each other in the horizontal direction, providing stable and vertical updraft for the mesocyclone, which enhances the suction of middle mesocyclone on the lower-level vortex and facilitates the formation of a tornado. At 18:30 on the 14th, the storm moved to the east of Taihu Lake, and the cold pool behind the storm was located in the center of the Taihu lake. Due to the large heat capacity of water, the temperature in the center of the cold pool was 26°C–27°C, with only a 2°C drop in temperature within an hour. The surrounding environment temperature was 28°C–29°C, and the temperature difference between the two was only 2°C. The intensity of the cold pool was not strong, which was favorable for the formation and maintenance of the tornado parent storm. At this time, the hook echo location was about 25 km southeast of the center of the cold pool (Figures 12E,F).

The thermal boundary of the lake surface was also the weather background for the occurrence of the tornado storm. The wind field

and temperature distribution of nearby ground automatic stations showed that there was no significant difference in temperature in the lake center and east bank at 17:30, and the thermal boundary was not obvious. From 18:00 to 18:30, the convective storm moved eastward to the east of Taihu Lake, and convective precipitation occurred on the lake from west to east. The temperature of the lake surface decreased, and the temperature difference between the east and the coast of the lake increased. The lake land breeze circulation could be seen on the wind field profile. A strong west-southwest wind and a high dew point temperature area from the lake surface were formed on the front side of the cold pool in the southeast of Taihu Lake and the east bank. The dew point temperature in the control area of the lake wind on the eastern bank of Taihu Lake had been relatively high, indicating strong water vapor transport by the lake wind, and the water vapor is replenished when the heavy precipitation supercell storm passed through the lake, providing favorable low-level water vapor conditions for the maintenance of storm intensity. When the storm meets the eastern bank lake wind, strong wind speed convergence and water vapor transport accumulation were very conducive to the uplift and strengthening of the front side of the storm. There was a continuous supply of strong southerly warm and humid air flow to the core of the storm, which maintains the intensity of the heavy rain supercell storm when passing through the Taihu Lake.

5.4 Baroclinity

At the time near the occurrence of the tornado, both the instability of atmospheric stratification and the wet baroclinity were significantly enhanced, which led to the strong development of cyclonic vorticity, providing extremely favorable dynamic conditions for the occurrence of the tornado. The evolution of relative humidity and temperature from the microwave radiometer over Kunshan Station on the 14th evening can further confirm that an unstable layer with dry and cold air above and warm and moist air below had formed over Suzhou before the tornado occurred (Figures 13A,B). From 18:00, the relative humidity decreased significantly from 1 to 3 km, and disturbances in water vapor density began to appear, indicating the dry air entrainment. From 18:30 to 19:00, as the tornado continued to develop downward, the dry layer near the ground extended upward to a height of 1.8 km, and the relative humidity rapidly increased to over 90% at a height of 1.8–5 km, with a significant increase in liquid water near a height of 1.5 km, with a central value exceeding 0.44 g/cm (Figures 13C,D). This indicates the existence of dry air entering the mid-to-high levels, which is conducive to the continuous evaporation of precipitation particles during the descent process, thus maintaining and strengthening the negative buoyancy of the downdraft. On the other hand, the unstable layer with dry air above and moist air below was further enhanced.

6 Conclusion

This paper analyzes the weather background, instability mechanism, and lifting conditions of an EF3 tornado that occurred in Shengze, Wujiang, Jiangsu on 14 May 2021. Using reanalysis data and wind field inversion from four radars, a detailed analysis of the internal structure of the tornado storm is conducted, and the following conclusions are obtained:

- (1) The tornado occurred in the warm and humid area inside the low-level shear line and the inverted trough at the surface, the southeast wind field to the east of the surface convergence line and high value area of water vapor flux on the left side of low altitude jet axis exit zone.
- (2) The intensity of the heavy rainfall supercell storm was strengthened after entering the Taihu Lake, and mesocyclones were detected with decreasing heights and increasing shear strengths which leading to the formation of the tornado parent storm. Tornado vortex storm (TVS) bottom height dropped to 0.3 km, the shear value increased to $169.1 \times 10^{-3}/s$, strong echoes above 60 dBZ reached to the ground, the difference between the lowest elevation Radial velocity (LLDV) and the maximum Radial velocity (MXDV) reached up to the largest value when tornado occurred.
- (3) The strong convergence of the ground and the enhancement of mesoscale frontal zone resulted in the strong development of thunderstorm cells. The deep rear inflow behind the heavy precipitation supercell storm passed through the stratiform cloud area and produced strong updraft due to the convergence of wind direction and wind speed. The updrafts generated vertical vorticity under the influence of wind shear, which was further stretched in the middle layer of the troposphere to form the core of the tornado.
- (4) The flat underlying surface, abundant water vapor, lake surface thermal boundary, and strong wind convergence on the east bank of Taihu Lake provided favorable conditions for the occurrence of the tornado. The centers of the mesocyclones in the lower and middle layers were close to each other in the horizontal direction, which provided stable and vertical updrafts for the mesocyclones and strengthened the suction effect of the mesocyclones on the low-level vortices, facilitating the formation of the tornado.

Data availability statement

The original contributions presented in the study are included in the article/Supplementary Material, further inquiries can be directed to the corresponding author.

Author contributions

SC led the conception and design of the paper. YW led the description and analysis of the case studies. JT and XZ led the literature review. RL, FW and YH provided Funding acquisition for the article. All authors contributed to the article and approved the submitted version.

Funding

This research supported by the Key Projects of Jiangsu Provincial Meteorological Bureau (KZ202108); Youth Innovation Team of China Meteorological Administration (CMA2023QN06); Basic Research Fund of CAMS (2021Z003); Key Projects of Jiangsu Provincial Meteorological Bureau (KZ202001).

Conflict of interest

The authors declare that the research was conducted in the absence of any commercial or financial relationships that could be construed as a potential conflict of interest.

Publisher's note

All claims expressed in this article are solely those of the authors and do not necessarily represent those of their affiliated organizations, or those of the publisher, the editors and the reviewers. Any product that may be evaluated in this article, or claim that may be made by its manufacturer, is not guaranteed or endorsed by the publisher.

References

- Bates, F. C. (1968). "A theory and model of the tornado," in *Proceeding of international conference on cloud physic* (Toronto: Amer Meteor Soc), 559–563.
- Bluestein, H. B., Thieme, K. J., Snyder, J. C., and Houser, J. B. (2019). Tornado genesis and early tornado evolution in the El Reno, Oklahoma, supercell on 31 May 2013. *Mon. Wea Rev.* 147 (6), 2045–2066. doi:10.1175/mwr-d-18-0338.1
- Brown, R. A., Lemon, L. R., and Burgess, D. W. (1978). Tornado detection by pulsed Doppler radar. *Mon. Wea Rev.* 106 (1), 29–38. doi:10.1175/1520-0493(1978)106<0029:tdbpdtr>2.0.co;2
- Browning, K. A., and Foote, G. B. (1976). Airflow and hail growth in supercell storms and some implications for hail suppression. *Quart. J. Roy. Meteor Soc.* 102 (433), 499–533. doi:10.1002/qj.49710243303
- Bruce, D. L., and Robert, B. W. (1997). The numerical simulation of non-supercell tornadogenesis. Part I: Initiation and evolution of pre-tornadic mesocyclone circulations along a dry outflow boundary. *J. Atmos. Sci.* 54 (1), 32–60. doi:10.1175/1520-0469(1997)054<0032:tnsons>2.0.co;2
- Doswell III, C. A., and Burgess, D. W. (1993). Tornadoes and toradoid storms: A review of conceptual models. C. Churc, D. Burgers, and C. Doswell, *The tornado: Its structure, dynamics, prediction, and hazards*. US: American Geophysical Union:161–172.
- Craven, J. P., and Brooks, H. E. (2004). Baseline climatology of sounding derived parameters associated with deep, moist convection. *Nat. Wea Dig.* 28, 13–24.
- Davies-Jones, R., Trapp, R. J., and Howard B Bluestein, H. B. (2001). "Tornadoes and tornadic storm," in *Doswell C A. Severe convective storms* (Boston: American Meteorological Society), 167–221.
- Doswell III, C. A. (2001). *Severe convective storms*. New York: American Meteorological Society.
- Duda, J. D., and Gallus, W. A., Jr (2010). Spring and summer Midwestern severe weather reports in supercells compared to other morphologies. *Wea Forecast.* 25 (1), 190–206. doi:10.1175/2009waf2222338.1
- Fan, W. J., and Yu, X. D. (2015). Characteristics of spatial temporal distribution of tornadoes in China. *Meteor Mon.* 41 (7), 793–805. doi:10.7519/j.issn.1000-0526.2015.07.001
- Feng, J. W., Min, J. Z., and Zhuang, X. R. (2017). The spatial and temporal distribution of Chinese tornadoes and their characteristics analysis of environmental physical variations. *J. Trop. Meteor.* 33 (4), 530–539. doi:10.16032/j.issn.1004-4965.2017.04.010
- Feng, J., Zhou, W. C., and Xu, Y. (2012). Change characters of tornadoes in China in 1980–2009. *Adv. Clim. Change Res.* 8 (3), 183–189. doi:10.3969/j.issn.1673-1719.2012.03.005
- Fujita, T. T. (1963). Analytical meso-meteorology: A review. Severe local storms. *Meteor Monogr.* 5 (27), 77–125.
- Fujita, T. T. (1971). *Proposed characterization of tornados and hurricanes by area and intensity*. Chicago: University of Chicago, 42.
- Fujita, T. T. (1987). *U.S. Tornadoes Part 1:70-Year statistics*. Chicago: University of Chicago, 122.
- Gao, S., and DaiXue, K. F. (2014). The design and development of grid edit platform based on MICAPS3.2 system. *Meteor Mon.* 40 (9), 1152–1158. doi:10.7519/j.issn.1000-0526.2014.09.013
- Grams, J. S., Thompson, R. L., Snively, D. V., Prentice, J. A., Hodges, G. M., and Reames, L. J. (2012). A climatology and comparison of parameters for significant tornado events in the United States. *Wea Forecast.* 27 (1), 106–123. doi:10.1175/waf-d-11-00008.1
- Jiang, L. J., Zou, H. B., Liu, Y. N., Li, B., and Liu, Y. Y. (2022). Radar echo characteristics and cause analysis of severe convective weather crossing Poyang Lake. *J. Subtropical Resour. Environ.* 17 (3), 41–48. doi:10.19687/j.cnki.1673-7105.2022.03.006
- Lemon, R. L., and Doswell III, C. A. (1979). Severe thunderstorm evolution and mesocyclones structure as related to tornadogenesis. *Mon. Wea Rev.* 107 (9), 1184–1197. doi:10.1175/1520-0493(1979)107<1184:STEAMS>2.0.CO;2
- Mao, Y., Li, L., Jiang, Y., Li, C., and Lu, M. X. Y. (2022). Analysis on the phase transformation of precipitation in a rain and snow event in spring. *Torrential Rain Disasters* 41 (3), 290–297. doi:10.3969/j.issn.1004-9045.2022.03.005
- Moller, A. R., Doswell III, C. A., Foser, M. P., and Woodall, G. R. (1994). The operational recognition of supercell thunderstorm environments and storm structures. *Wea Forecast.* 9 (3), 327–347. doi:10.1175/1520-0434(1994)009<0327:torost>2.0.co;2
- Mu, R. Q., Wu, H. Y., Li, Y., Wang, X. H., Lv, R. Q., and Sun, K. Y. (2021). Analysis of EF2~EF3 tornado weather in northern Jiangsu on July 22, 2020. *J. Trop. Meteorology* 37 (5/6), 759–769. doi:10.16032/j.issn.1004-4965.2021.070
- Potvin, J., Goldbogen, J. A., and Shadwick, R. E. (2012). Metabolic expenditures of lunge feeding orcas across scale: implications for the evolution of filter feeding and the limits to maximum body size. *PLoS ONE* 7, e44854. doi:10.1371/journal.pone.0044854
- Ray, P. S., Doviak, R. J., Walker, G. B., Sirmans, D., Carter, J., and Bumgarner, B. (1975). Dual-Doppler observation of a tornadic storm. *J. Appl. Meteor.* 14 (8), 1521–1530. doi:10.1175/1520-0450(1975)014<1521:DDOAT>2.0.CO;2
- Shen, F., Min, J., and Xu, D. (2016). Assimilation of radar radial velocity data with the WRF Hybrid ETKF--3DVAR system for the prediction of Hurricane Ike (2008). *Atmos. Res.* 169, 127–138. doi:10.1016/j.atmosres.2015.09.019
- Shen, F., Song, L., Li, H., He, Z., and Xu, D. (2022). Effects of different momentum control variables in radar data assimilation on the analysis and forecast of strong convective systems under the background of northeast cold vortex. *Atmos. Res.* 280, 106415. doi:10.1016/j.atmosres.2022.106415
- Shen, F., Xu, D., Min, J., Chu, Z., and Li, X. (2020). Assimilation of radar radial velocity data with the WRF Hybrid 4DVar system for the prediction of Hurricane Ike (2008). *Atmos. Res.* 230, 104771. doi:10.1016/j.atmosres.2019.104771
- Shu, A., Shen, F., Jiang, L., Zhang, T., and Xu, D., (2022). Assimilation of Clear-sky FY-4A AGRI radiances within the WRFDA system for the prediction of a landfalling Typhoon Hagupit. *Atmos. Res.* 283, 106556. doi:10.1016/j.atmosres.2022.106556
- Smith, B. T., Thompson, R. L., Grams, J. S., Broyles, C., and Brooks, H. E. (2012). Convective modes for significant severe thunderstorms in the contiguous United States. Part I: Storm classification and climatology. *Wea Forecast.* 27 (5), 1114–1135. doi:10.1175/waf-d-11-00115.1
- Song, L., Shen, F., Shao, C., Shu, A., and Zhu, L. (2022). Impacts of 3DVar-based FY-3D MWHS-2 radiance assimilation on numerical simulations of landfalling typhoon ampil (2018). *Remote Sens.* 14, 6037. doi:10.3390/rs14236037
- Wang, Y., Zheng, Y. Y., Sun, K. Y., and Wu, H. Y. (2018). Statistical analysis of characteristic values of mesocyclone products of nanjing radar. *J. Meteorology* 76 (2), 266–278. doi:10.11676/qxb2017.087
- Wei, W. X., and Zhao, Y. M. (1995). The characteristics of tornadoes in China. *Meteor. Mon.* 21 (5), 36–40. (in Chinese).
- Wen, H., Liu, L. P., Zhang, C. A., Yin, C. G., Zhang, Y., and Shi, C. (2016). Operational evaluation of radar data quality control for ground clutter and electromagnetic interference. *J. Meteorological Sci.* 36 (6), 789–799. doi:10.3969/2015jms.0085
- Wu, H. Y., Shen, S. Q., Jiang, Y. F., Wang, W. F., and Zhou, Q. J. (2009). Example analysis of the causes of tornadoes. *Meteorological Sci.* 29 (3), 335–341.
- Xu, F., Zheng, Y. Y., and Sun, K. Y. (2021). The spatiotemporal distribution and storm morphology characteristics of tornadoes in Jiangsu. *Meteorology* 47 (5), 517–528. doi:10.7519/j.issn.1000-0526.2021.05.001
- Xu, X. Z., Pan, W. Z., and Miao, Q. L. (2010). Vulnerability analysis of tornado disaster in Jiangsu. *Sci. Meteor Sin.* 30 (2), 208–213.
- Xue, D. Q., and Yang, C. F. (2003). Features of tornadoes distribution in shandong Province. *J. Shandong Meteor* 23 (4), 9–11.
- Yao, Y. Q., Yu, X. D., Zhang, Y. J., Zhou, Z. J., Xie, W. S., Lu, Y. Y., et al. (2015). Climate analysis of tornadoes in China. *J. Meteor. Res.* 29 (3), 359–369. doi:10.1007/s13351-015-4983-0
- Yu, X. D., Zhao, J., and Fan, W. J. (2021). The spatiotemporal distribution and key environmental parameter characteristics of Chinese tornadoes. *J. Trop. Meteorology* 37 (5/6), 681–692. doi:10.16032/j.issn.1004-4965.2021.064
- Zeng, M. J., Wu, H. Y., Wang, X. F., and Jiang, Y. F. (2016). Analysis of the environmental conditions and structural characteristics of typical tornado convective storms during the Mei-yu period. *Meteorology* 42 (3), 280–293. doi:10.7519/j.issn.1000-0526.2016.3.003
- Zhang, X. L., Yang, B., Zhu, W. J., Fang, C., Liu, X. H., Zhou, K. H., et al. (2016). Weather analysis of an EF4 tornado in funing, Jiangsu on June 23, 2016. *Meteorology* 42 (11), 1304–1314. doi:10.7519/j.issn.1000-0526.2016.11.002
- Zhang, X., Xu, D., Liu, R., and Shen, F. (2022). Impacts of FY-4A AGRI radiance data assimilation on the forecast of the super typhoon "in-fa" (2021). *Remote Sens.* 14, 4718. doi:10.3390/rs14194718
- Zheng, Y. G., Zhu, W. J., and Yao, D. (2016). Wind speed level standards and estimation of the intensity of the Funing tornado on June 23, 2016. *Meteorology* 42 (11), 1289–1303. doi:10.7519/j.issn.1000-0526.2016.11.001